CHIN. PHYS. LETT. Vol. 37, No. 5 (2020) 058501

Ultrafast Magnetization Precession in Perpendicularly Magnetized $L1_0$-MnAl Thin Films with Co_2MnSi Buffer Layers *

Si-Wei Mao(毛思玮)[1,2], Jun Lu(鲁军)[3], Long Yang(杨龙)[4], Xue-Zhong Ruan(阮学忠)[4], Hai-Long Wang(王海龙)[1,2], Da-Hai Wei(魏大海)[1,2,3], Yong-Bing Xu(徐永兵)[4], Jian-Hua Zhao(赵建华)[1,2,3]**

[1]*State Key Laboratory of Superlattices and Microstructures, Institute of Semiconductors, Chinese Academy of Sciences, Beijing 100083*

[2]*Center of Materials Science and Optoelectronics Engineering, University of Chinese Academy of Sciences, Beijing 100190*

[3]*Beijing Academy of Quantum Information Science, Beijing 100193*

[4]*Jiangsu Provincial Key Laboratory of Advanced Photonic and Electronic Materials, Collaborative Innovation Center of Advanced Microstructures, School of Electronic Science and Engineering, Nanjing University, Nanjing 210093*

(Received 17 January 2020)

Perpendicularly magnetized $L1_0$-MnAl thin films with Co_2MnSi buffer layers were prepared on GaAs (001) substrates by molecular-beam epitaxy (MBE). The samples with high crystalline quality show a maximum uniaxial perpendicular magnetic anisotropy constant of 1.4×10^7 erg/cm^3. Ultrafast spin dynamics with a magnetization precession frequency up to 200 GHz was investigated by using time-resolved magneto-optical Kerr effect (TRMOKE) measurements, from which the Gilbert damping constant α of epitaxial $L1_0$-MnAl thin films is evaluated to be less than 0.0175. This work provides an important reference for analyzing the current-induced magnetization switching process in MnAl-based spintronic devices.

PACS: 85.75.−d, 46.40.Ff, 75.30.Gw DOI: 10.1088/0256-307X/37/5/058501

Tetragonal Mn-based binary alloys, including $L1_0$-MnGa, $D0_{22}$-MnGa and $L1_0$-MnAl, have drawn broad concern in recent years owing to their huge bulk perpendicular magnetic anisotropy (PMA), high spin polarization P, high Curie temperature T_C and relative low saturation magnetization M_s.[1−11] These advantages make them perfect candidates for free layers in the fabrication of perpendicular magnetic tunnel junctions (p-MTJs),[12−16] which are regarded as the core memory cells of spin-transfer-torque magnetoresistance random access memory (STT-MRAM).[17−19] Particularly, in an STT system, there is another key factor to be considered, namely, Gilbert damping constant α. As defined in the Landau–Lifshitz–Gilbert (LLG) equation,[20] α evaluates the relaxation rate of magnetization precession. This factor has great impacts on not only the operating speed but also the power consumption of current-induced magnetization switching.[19] Thus, research of the spin dynamics and determination of the experimental α values of Mn-based binary alloys are quite significant for anticipating the performance of related spintronic devices.

In perpendicularly magnetized ferromagnetic thin films, the Larmor precession frequency can be expressed as $f = \frac{\gamma}{2\pi} H_K^{\text{eff}}$,[21] where H_K^{eff} represents the effective PMA field and γ is the gyromagnetic ratio. For MnGa and MnAl alloys with very strong PMA ($K_u \sim 10^7$ erg/cm^3), H_K^{eff} is always dozens of kOe and the corresponding f may reach one hundred to several hundreds of GHz. Unfortunately, magnetization precession at such a high frequency is hard to detect by means of conventional microwave ferromagnetic resonance (FMR) since compatible microwave sources are not commonly used. One alternative solution is to use the time-resolved magneto-optical Kerr effect (TRMOKE). TRMOKE is an all-optical measurement technique, in which the pump and probe of magnetization precession are realized by femtosecond laser pulses. The advantage of TRMOKE is that it enables us to explore the spin dynamics in a broader range of frequency, especially in high frequency region. Benefit from this powerful technique, Gilbert damping in MnGa thin films has been systematically investigated by Mizukami's group.[22−23] According to their study, the α values of $L1_0$-MnGa and $D0_{22}$-MnGa are not greater than 0.008 and 0.015, respectively.[22] However, as far as we know, relevant experimental researches on $L1_0$-MnAl system are still absent up to now.

In this Letter, $L1_0$-ordered MnAl thin films were prepared on GaAs (001) substrates by molecular-beam epitaxy (MBE). In order to restrict the atomic interdiffusion at the initial GaAs/MnAl interface, ultrathin Co_2MnSi inserts (< 1 nm) were used as buffer layers. As a result, the samples have high crystalline quality and show a strong PMA. Furthermore, ultrafast magnetization precession process in $L1_0$-MnAl thin films was investigated by using TRMOKE measurements combined with an electromagnet with a maximum field of 20 kOe. The effective damping constant

*Supported by the National Key R&D Program of China (Grant No. 2018YFB0407601), the Key Research Project of Frontier Science of Chinese Academy of Sciences (Grant Nos. QYZDY-SSW-JSC015 and XDPB12), and the National Natural Science Foundation of China (Grant Nos. 11834013, 11874349, and 11774339).

**Corresponding author. Email: jhzhao@red.semi.ac.cn

© 2020 Chinese Physical Society and IOP Publishing Ltd

($\alpha_{\rm eff}$) of $L1_0$-MnAl thin films was determined experimentally for the first time.

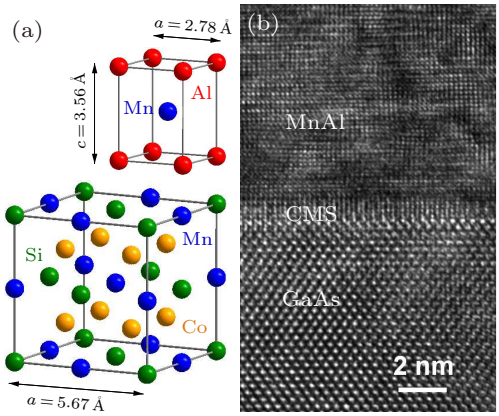

Fig. 1. (a) Schematic diagram of the crystal structures of $L1_0$-ordered MnAl and $L2_1$-ordered Co_2MnSi (CMS). (b) Cross-sectional HRTEM image of the $L1_0$-MnAl thin film deposited on the GaAs (001) substrate with a Co_2MnSi buffer layer.

$L1_0$-MnAl is the only ferromagnetic phase of Mn–Al alloy system. It has a tetragonal CuAu type-I structure with Mn and Al monolayers stacked alternatively along the c-axis, as shown in Fig. 1(a). To prepare $L1_0$-MnAl thin films on Ⅲ–Ⅴ compound semiconductors such as GaAs, the so-called template technique is usually used,[9,11,24] i.e., an ultrathin amorphous MnAl template layer (< 0.5 nm) is firstly deposited onto the substrate at room temperature to inhibit the interfacial reactions, then it is crystallized into $L1_0$-ordered structure by subsequent annealing process at 200–300 ℃, after which the deposition of the MnAl thin film is followed at optimal temperature (∼350℃). In this approach, the acquisition of high-quality MnAl template is crucial since it is the seed layer for subsequent epitaxial growth. However, the crystallization procedure of the template is very sensitive to both the annealing temperature and the layer component. Once hexagonal ε-MnAl or MnAs second phases are formed during the heat treatment, the whole epitaxial structure may be disrupted. To solve this problem, a new growth method is proposed here by inserting a 0.8 nm Co_2MnSi buffer layer between MnAl and the GaAs substrate. Co_2MnSi thin films (the crystal structure is shown in Fig. 1(a)) are easy to crystallize on GaAs (001) at the deposition temperature of 250 ℃, therefore a perfect metallic type surface can be obtained after the buffer deposition. Moreover, the lattice constants of cubic Co_2MnSi and GaAs are nearly the same, hence no additional lattice mismatch would be introduced. Consequently, MnAl thin films can be prepared directly on Co_2MnSi at 350 ℃ with good repeatability. Figure 1(b) shows the cross-section high-resolution transmission electron microscopy (HRTEM) image of a typical MnAl thin film with a Co_2MnSi buffer layer. As we can see, GaAs/Co_2MnSi/MnAl trilayers are epitaxially grown along the [001] direction. Sharp interfaces among each layer can be clearly identified, which proves that the currently used growth conditions are appropriate.

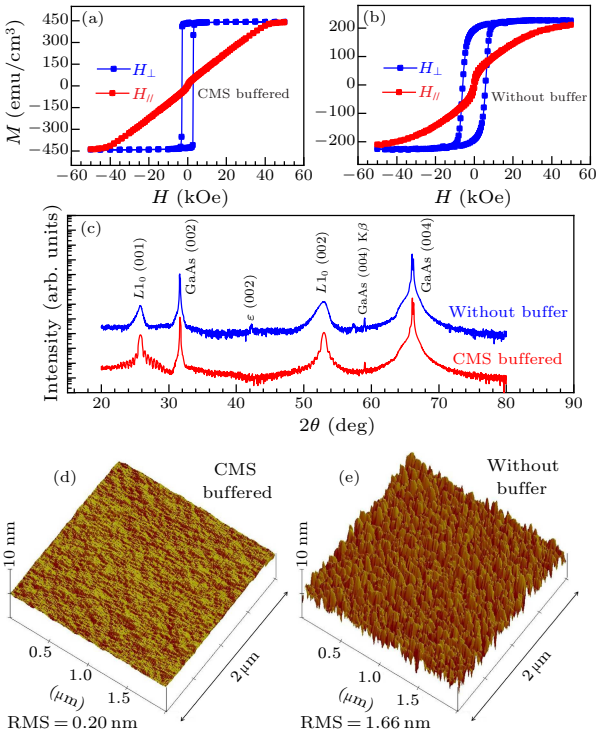

Fig. 2. Hysteresis loops of 30 nm $L1_0$-$Mn_{52}Al_{48}$ thin films prepared (a) with and (b) without Co_2MnSi (CMS) buffers. (c) XRD θ–2θ patterns. AFM images of $L1_0$-$Mn_{52}Al_{48}$ thin films (d) with and (e) without Co_2MnSi buffers.

MnAl thin films with and without Co_2MnSi buffers were prepared on GaAs (001) substrates for comparison. The sample structures are GaAs sub/Co_2MnSi buffer (0.8 nm)/$Mn_{52}Al_{48}$ (30 nm)/Pt cap (2 nm) and GaAs sub/MnAl template (0.4 nm)/$Mn_{52}Al_{48}$ (30 nm)/Pt cap (2 nm), respectively. Figures 2(a) and 2(b) depict their in-plane and out-of-plane hysteresis loops measured by superconducting quantum interference device (SQUID) magnetometer, from which we can confirm that these two samples exhibit distinct PMA. Specifically, the sample with the Co_2MnSi buffer layer shows a more square out-of-plane loop and its saturation magnetization $M_{\rm s}$ (440 emu/cm^3) is much larger than the one without Co_2MnSi buffer (230 emu/cm^3). Meanwhile, the uniaxial PMA constant $K_{\rm u}$ (estimated by $K_{\rm u} = \frac{H_{\rm s}M_{\rm s}}{2} + 2\pi M_{\rm s}^2$) of the former sample ($1.1 \times 10^7$ erg/cm^3) is also higher than that of the latter one (7.1×10^6 erg/cm^3). To explain these differences, further structural analysis was carried out by x-ray diffraction (XRD) measurement. As shown in Fig. 2(c), besides the diffraction peaks from GaAs substrates, (001) and (002) peaks of $L1_0$-ordered MnAl are marked in the figure. The full width at half maximum (FWHM) of the MnAl (002) peak in the Co_2MnSi buffered sample is 0.62°. However, this value is 1.20° in the sample without buffer. The above

observations indicate that higher crystalline quality was achieved in the Co_2MnSi buffered MnAl thin film, which is closely related to the sample preparation method. The single-crystalline Co_2MnSi buffer layer offers a smooth metallic surface for subsequent epitaxial growth, so that the Mn and Al atoms can easily migrate to their equilibrium positions. Highly ordered atomic arrangement leads to a squared M–H loop and strong PMA. In contrast, the amorphous MnAl template deposited on the GaAs substrate was crystallized by annealing process. During this procedure, the interfacial atomic diffusion as well as the surface energy difference between semiconductors and metals may introduce defects at the initial interface, usually in the form of dislocations or atomic substitutions. Subsequently, these interfacial defects may extend into the MnAl thin films, resulting in the degraded crystalline quality and lower PMA. Moreover, a small (002) peak of paramagnetic ε-phase MnAl is found in the XRD pattern of the unbuffered sample, which is another evidence for its small M_s. In addition, the morphology of these two samples was characterized by using atomic force microscope (AFM), as shown in Figs. 2(d) and 2(e). The Co_2MnSi buffered sample has a flat surface with the rms roughness of 0.2 nm, while a much larger rms roughness of 1.66 nm was observed in the sample without buffer. This reveals that relatively larger crystalline grains were generated by using the template growth method, which may limit its application in practical devices such as MTJs.

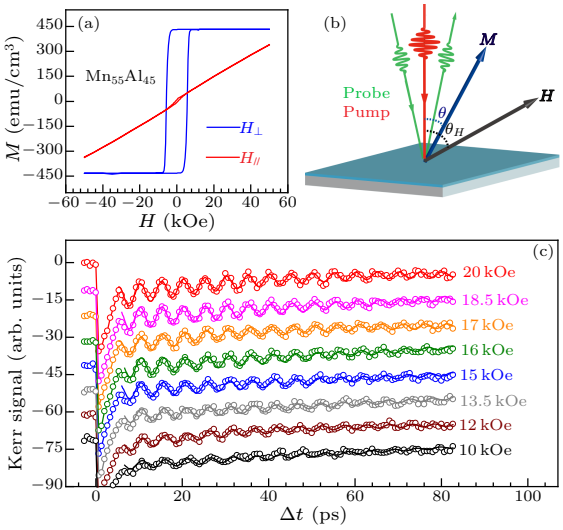

Fig. 3. (a) In-plane and out-of-plane hysteresis loops of a 65 nm thick $L1_0$-$Mn_{55}Al_{45}$ thin film with 0.8 nm Co_2MnSi buffer layer. (b) Schematic diagram of the TRMOKE measurements. In the present case, θ_H is fixed to 60°. (c) Time-resolved Kerr signal for the 65 nm $L1_0$-$Mn_{55}Al_{45}$ thin film under different external fields H. The open circles show the experimental data and the solid curves depict the fitted Kerr traces.

After optimizing the preparation method of $L1_0$-MnAl thin films, the spin dynamics was investigated. $L1_0$-MnAl thin films prepared with Co_2MnSi buffer layers show higher crystalline quality, better morphology and larger PMA, which can avoid the impacts of sample inhomogeneity to the greatest extent during the TRMOKE measurements. Furthermore, in order to suppress the Kerr signals of Co_2MnSi buffer and get rid of the interference induced by spin pumping effect at MnAl/Pt interface, a thicker $L1_0$-MnAl sample with the structure of GaAs sub/Co_2MnSi (0.8 nm)/$Mn_{55}Al_{45}$(65 nm)/Pt cap (2 nm) was selected (the probing depth of TRMOKE is normally 10–20 nm in most metals[25]). Figure 3(a) displays the hysteresis loops measured at room temperature. By extrapolating the in-plane loop to cross it with the out-of-plane one, we can estimate K_u of the current sample reaching 1.4×10^7 erg/cm^3.

Figure 3(b) shows the schematic diagram of currently used TRMOKE measurement. Linearly polarized pump and probe beams generated from the Ti:sapphire regenerative amplifier were focused on the sample surface with spot diameters of 500 μm and 200 μm. The central wavelength, repetition rate and pulse width of the laser were 800 nm, 1 kHz and 60 fs, respectively. The pump beam was incident almost perpendicularly onto the sample surface while the probe beam was settled at an incidence angle of 3°. Additionally, an external field H was applied along $\theta_H = 60°$ relative to the normal direction to tilt the equilibrium magnetization M away from its easy axis by θ.

Collective spins of the sample will be triggered out of equilibrium after the pump pulse absorption, which is regarded as an ultrafast demagnetization process. Subsequently, the magnetization was quickly restored and began to precess around the effective field consisting of both the external field and the PMA effective field. Then the amplitude of magnetization oscillation gradually decayed under the influence of Gilbert damping and finally relaxed to the equilibrium state. This damped precession process can be recorded by the Kerr signal of the reflected probe beam since it is very sensitive to the normal component of the magnetization. The open circles in Fig. 3(c) depict the traces of the Kerr signal ($\Delta\Phi_k$) with respect to the delay time (Δt) between pump and probe. During the measurements, external fields with various intensities between 10 kOe to 20 kOe were applied. The variation of H may modulate the vertical projection of M as well as the shape of the precession orbit, and further change the amplitude and oscillation frequency of $\Delta\Phi_k$. Kerr traces were fitted by a phenomenological formula:[21–23,26]

$$\Delta\Phi_k = Ae^{-\frac{\Delta t}{\tau}}\sin(2\pi f\Delta t + \phi_0) + Be^{-\frac{\Delta t}{\tau_0}} + C. \quad (1)$$

The first term on the right side represents the decayed precession of the magnetization, the last two terms describe the magnetization recovery procedure and background signals, respectively. A, B, C are the amplitude of each contribution, and f, τ, τ_0, and

ϕ_0 are the frequency, relaxation time, recovery time, and initial phase of the magnetization precession, respectively. As shown by the solid lines in Fig. 3(c), our fitting curves coincide well with the experimental data. By fitting the Kerr traces, these parameters can be accurately extracted.

To quantitatively analyze the spin dynamics in $L1_0$-MnAl thin films, the dependence of precession frequency (f) on external field (H) was calculated by using Kittel's equation,[22,27,28] which is derived from the LLG equation under the linear approximation of uniform magnetization precession around the equilibrium direction with small cone angle:

$$f = \frac{\gamma}{2\pi}\sqrt{H_1 \cdot H_2}, \tag{2}$$

$$H_1 = H\cos(\theta_H - \theta) + H_{\rm K}^{\rm eff}\cos^2\theta, \tag{3}$$

$$H_2 = H\cos(\theta_H - \theta) + H_{\rm K}^{\rm eff}\cos(2\theta), \tag{4}$$

where $H_{\rm K}^{\rm eff}$ is the effective PMA field defined as $H_{\rm K}^{\rm eff} = H_{\rm K} - 4\pi M_{\rm s}$, γ is the gyromagnetic ratio defined as $\gamma \equiv g\mu_{\rm B}/\hbar$. The relationship between θ and H can be determined from the expression:[22,28]

$$\sin(2\theta) = \frac{2H}{H_{\rm K}^{\rm eff}}\sin(\theta_H - \theta). \tag{5}$$

Here an effective PMA field $H_{\rm K}^{\rm eff} \approx 62$ kOe was estimated from the hysteresis loop (Fig. 3(a)) and Lande's g factor was fixed to the same value with free electrons ($g \approx 2.0$). Figure 4(a) shows the calculated curve (solid line) and the experimental values (open circles) of f versus H. The experimental values agree well with the calculated curve, suggesting that our experimental results are highly reliable.

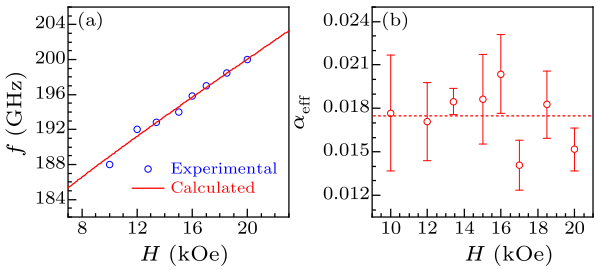

Fig. 4. (a) Precession frequency f as a function of the external field H. Open circles show the experimental values and the solid curve is theoretical result calculated by using Kittle's equation. (b) Effective damping constant $\alpha_{\rm eff}$ determined under different external fields H. The dashed line marks the average value of 0.0175.

Finally, the effective damping constants ($\alpha_{\rm eff}$) under each applied field were determined using the relation[22,29]

$$\alpha_{\rm eff} = \frac{1}{2\pi f\tau}. \tag{6}$$

As shown in Fig. 4(b), the dashed line marks the average $\alpha_{\rm eff}$ value of 0.0175. It is worth noting that $\alpha_{\rm eff}$ is frequently used to analyze the spin relaxation process in ferromagnetic thin films because it can be obtained directly from the experimental values (f and τ) without considering the analytical models. Nevertheless, $\alpha_{\rm eff}$ is not equal to the intrinsic Gilbert damping constant α_0. Besides the intrinsic component, $\alpha_{\rm eff}$ also contains the contribution of extrinsic damping mechanisms, which are usually considered to originate from the magnetic anisotropy dispersion in the sample or the multiple-mode spin wave excitations.[22,30,31] The extrinsic mechanism may cause extra damping-enhanced precession process, thus $\alpha_{\rm eff}$ gives only the upper limit of α_0. Normally, the intrinsic damping does not change with the external field H while the extrinsic damping does,[29] implying that $\alpha_{\rm eff}$ should have a distinct dependence on H if the extrinsic mechanism plays a major role. However, from Fig. 4(b) we can see that the values of $\alpha_{\rm eff}$ fluctuate in a narrow range from 0.014 to 0.021 and show no remarkable dependence on H within the experimental errors, which demonstrates that the extrinsic damping is not dominating in the present case. The above discussions indicate that the damping constant of the current $L1_0$-MnAl thin films is not greater than 0.0175 and the approximate evaluations using $\alpha_{\rm eff}$ are reasonable. The $\alpha_{\rm eff}$ in $L1_0$-MnAl is larger than that of $L1_0$-MnGa (0.008),[22] while is comparable to other commonly used PMA thin films such as $D0_{22}$-MnGa (0.015)[22] and ultrathin CoFeB/MgO ($0.01 \sim 0.02$).[32,33]

In conclusion, perpendicularly magnetized $L1_0$-MnAl thin films have been prepared on GaAs (001) substrates and the relevant magnetization precession process has been studied using TRMOKE measurements. By inserting ultrathin Co_2MnSi buffer layers between MnAl and GaAs, the initial interfaces are obviously optimized. Consequently, a small rms roughness of 0.2 nm and maximum $K_{\rm u}$ of 1.4×10^7 erg/cm^3 are achieved in the current samples. Resulting from the huge PMA, the ultrafast magnetization precession with a frequency up to 200 GHz is observed. For the first time, the effective Gilbert damping constant $\alpha_{\rm eff}$ of $L1_0$-MnAl thin films is experimentally determined to be $\sim$0.0175, which is comparable to other commonly used PMA materials. These results demonstrate that $L1_0$-MnAl has a great potential for practical applications in related spintronic devices, such as perpendicular magnetic tunnel junctions or spin nano-oscillators.

References

[1] Zhu L J, Nie S H, Meng K K, Pan D, Zhao J H and Zheng H Z 2012 *Adv. Mater.* **24** 2547
[2] Winterlik J, Balke B, Fecher G H and Felser C 2008 *Phys. Rev. B* **77** 054406
[3] Zhu L J and Zhao J H 2013 *Appl. Phys. A* **111** 379
[4] Balke B, Fecher G H, Winterlik J and Felser C 2007 *Appl. Phys. Lett.* **90** 152504
[5] Kurt H, Rode K, Venkatesan M, Stamenov P and Coey J M D 2011 *Phys. Rev. B* **83** 020405(R)
[6] Park J H, Hong Y K, Bae S, Lee J J, Jalli J, Abo G S, Neveu N, Kim S G, Choi C J and Lee J G 2010 *J. Appl.*

Phys. **107** 09A731
[7] Edstrom A, Chico J, Jakobsson A, Bergman A and Rusz J 2014 *Phys. Rev. B* **90** 014402
[8] Zeng Q, Baker I, Cui J B and Yan Z C 2007 *J. Magn. Magn. Mater.* **308** 214
[9] Sands T, Harbison J P, Leadbeater M L, Allen S J, Hull G W, Ramesh R and Keramidas V G 1990 *Appl. Phys. Lett.* **57** 2609
[10] Oogane M, Watanabe K, Saruyama H, Hosoda M, Shahnaz P, Kurimoto Y, Kubota M and Ando Y 2017 *Jpn. J. Appl. Phys.* **56** 0802A2
[11] Nie S H, Zhu L J, Lu J, Pan D, Wang H L, Yu X Z, Xiao J X and Zhao J H 2013 *Appl. Phys. Lett.* **102** 152405
[12] Ma Q L, Kubota T, Mizukami S, Zhang X M, Naganuma H, Oogane M, Ando Y and Miyazaki T 2012 *Appl. Phys. Lett.* **101** 032402
[13] Kubota T, Mizukami S, Watanabe D, Wu F, Zhang X M, Naganuma H, Oogane M, Ando Y and Miyazaki T 2011 *J. Appl. Phys.* **110** 013915
[14] Suzuki K Z, Miura Y, Ranjbar R, Sugihara A and Mizukami S 2018 *J. Phys. D* **51** 235001
[15] Saruyama H, Oogane M, Kurimoto Yuta, Naganuma H and Ando Y 2013 *Jpn. J. Appl. Phys.* **52** 063003
[16] Mao S W, Lu J, Wang H L, Zhao X P, Wei D H and Zhao J H 2019 *J. Phys. D* **52** 405002
[17] Kent A D and Worledge D C 2015 *Nat. Nanotechnol.* **10** 187
[18] Wang K L, Alzate J G and Amiri P K 2013 *J. Phys. D* **46** 074003
[19] Khvalkovskiy A V, ApalKov D, Watts S, Chepulskii R, Beach R S, Ong A, Tang X, Driskill-Smith A, Butler W H, Visscher P B, Lottis D, Chen E, Nikitin V and Krounbi M 2013 *J. Phys. D* **46** 139601
[20] Gilbert T L 2004 *IEEE Trans. Magn.* **40** 3443
[21] Mizukami S, Iihama S, Sakaki Y, Sugihara A, Ranjbar R and Suzuki K Z 2016 *J. Appl. Phys.* **120** 142102
[22] Mizukami S, Wu F, Sakuma A, Walowski J, Watanabe D, Kubota T, Zhang X, Naganuma H, Oogane M, Ando Y and Miyazaki T 2011 *Phys. Rev. Lett.* **106** 117201
[23] Mizukami S, Suzuki K Z and Miura Y 2019 *Appl. Phys. Express* **12** 043003
[24] Harbison J P, Sands T, Ramesh R, Florez L T, Wilkens B J and Keramidas V G 1991 *J. Cryst. Growth* **111** 978
[25] Bland J A C, Padgett M J, Butcher R J and Bett N 1989 *J. Phys. E* **22** 308
[26] Qiao S, Nie S H, Zhao J H and Zhang X H 2014 *Appl. Phys. Lett.* **105** 172406
[27] Mizukami S, Abe H, Watanabe D, Oogane M, Ando Y and Miyazaki T 2008 *Appl. Phys. Express* **1** 121301
[28] Mizukami S, Ando Y and Miyazaki T 2001 *Jpn. J. Appl. Phys.* **40** 580
[29] Mizukami S, Watanabe D, Kubota T, Zhang X M, Naganuma H, Oogane M, Ando Y and Miyazaki T 2010 *Appl. Phys. Express* **3** 123001
[30] Serrano-Guisan S, Rott K, Reiss G and Schumacher H W 2008 *J. Phys. D* **41** 164015
[31] Beaujour J M, Ravelosona D, Tudosa I, Fullerton E E and Kent A D 2009 *Phys. Rev. B* **80** 180415(R)
[32] Devolder T, Ducrot P H, Adam J P, Barisic I, Vernier N, Kim J V, Ockert B and Ravelosona D 2013 *Appl. Phys. Lett.* **102** 022407
[33] Iihama S, Mizukami S, Naganuma H, Oogane M, Ando Y and Miyazaki T 2014 *Phys. Rev. B* **89** 174416